Steady-State dc and Impedance Investigations of H_2/O_2 Alkaline Membrane Fuel Cells with Commercial Pt/C, Ag/C, and Au/C Cathodes

John R. Varcoe,*,† Robert C. T. Slade,† Graham L. Wright,† and Yanling Chen‡

Department of Chemistry and Microstructural Studies Unit (MSSU), School of Engineering, The University of Surrey, Guildford GU2 7XH, United Kingdom

Received: July 31, 2006; In Final Form: August 21, 2006

The performances of H_2/O_2 metal−cation−free alkaline anion-exchange membrane (AAEM) fuel cells operated with commercially available Au/C and Ag/C cathodes are reported for the first time. Of major significance, the power density obtained with 4 mg cm^{-2} Ag/C (60% mass) cathodes was comparable to that obtained with 0.5 mg cm^{-2} Pt/C (20% mass) electrodes, whereas the performance when using the same Ag/C cathode in a Nafion-based acidic membrane electrode assembly (MEA) was poor. These initial studies demonstrate that the oxygen reduction electrokinetics are improved when operating Pt/C cathodes at high pH in AAEM-based fuel cells as compared with operation at low pH (in Nafion-based proton-exchange membrane fuel cells). The results of in situ alternating current impedance spectroscopy were core to the assignment of the source of the limited performances of the AAEM-based fuel cells as being the limited supply of water molecules to the cathode reaction sites. Minimizing the thickness of the AAEM improved the performances by facilitating back-transport of water molecules from the anode (where they are generated) to the cathode. The urgent need for development of electrode architectures that are specifically designed for use in AAEM-based fuel cells is highlighted.

1. Introduction

The growing interest in the application of alkaline anion-exchange membranes (AAEM) in metal−cation−free solid-state alkaline fuel cells (AFC) is principally motivated by the prospective use of cheap and relatively abundant non-Pt electrocatalysts. Simple Ag/C and Au/C catalysts represent promising oxygen reduction reaction (ORR) catalysts in high-pH media.[1] The "acid stability criterion" precludes the use of such non-noble metal catalysts in the acidic environment found in proton-exchange membrane fuel cells (PEMFCs).[2] Voltammetric studies have confirmed that Ag [3] and Au [4] surfaces catalyze the ORR in aqueous alkali via a $4e^-$-serial mechanism, with very little production of undesirable H_2O_2. $4e^-$ ORR has also been reported on carbon-supported nanoparticulate Ag and Au catalysts in alkali;[1,5] consideration must, however, be given to H_2O_2 production anticipated at high pH due to the carbon supports.[6] Countanceau et al.[7] have investigated Ag/C catalysts for use in direct alcohol alkaline membrane fuel cells and concluded that $4e^-$ ORR was predominant. The power performances of alkaline membrane direct ethylene glycol fuel cells (KOH added to aqueous ethylene glycol supply: K^+ cations are present) were comparable when Ag/C and Pt/C cathode catalysts were evaluated.[8] Cathodes containing Ag/C catalysts,[9] along with cheap Ni-based anodes,[10] are widely and successfully employed in traditional aqueous KOH electrolyte (nonmembrane) AFCs, where the only significant concern is catalyst durability in the highly caustic aqueous environment.

A recent review discusses the application of AAEMs in fuel cells in detail.[11] Widely perceived problems with AAEMs include the following: (1) low conductivity,[12] (2) low thermal and chemical stability (especially the stability of the quaternary ammonium functional groups toward the nucleophillic displacement by the hydroxide anions), and (3) undesirable formation of carbonate species, from the reaction between CO_2 and OH^- when operated in AFCs with air cathodes (consequential drops in pH and reductions in ionic conductivity of the electrolyte). In response to these concerns, preliminary studies on quaternary-ammonium-based radiation-grafted AAEMs have shown that (1) conductivities in water at 50 °C are 20−33% of the values observed with Nafion-115 proton-exchange membrane (PEM), which is entirely adequate for application in fuel cells;[13] (2) OH^- contents (ion-exchange capacities, IEC) are retained with the AAEMs immersed in water at 60 °C for several thousand hours;[14] (3) the OH^- content and fuel cell performance of a metal−cation−free AAEM−membrane electrode assembly (AAEM-MEA) is stable when tested in a methanol/air fuel cell for more than 230 h at 50 °C (even though CO_2 is constantly generated at the anode from methanol electrooxidation and supplied to the cathode as a component of air).[15] Sata et al. also report that AAEMs based around quaternary ammonium functionality exhibit notable stability when immersed in concentrated aqueous solutions of alkali metal hydroxides at elevated temperatures.[16]

The fuel cell reactions for an AAEM fuel cell with H_2 anode supply and O_2 cathode supply are

$$\text{anode: } H_2(g) + 2OH^-(\text{membrane}) \rightarrow 2H_2O(l/g) + 2e^- \quad (1)$$

$$\text{cathode: } H_2O(g/l) + {}^1/_2O_2(g) + 2e^- \rightarrow 2OH^-(\text{membrane}) \quad (2)$$

$$\text{overall: } H_2(g) + {}^1/_2O_2(g) \rightarrow H_2O(l/g) \quad (3)$$

The cell reactions at the electrodes are significantly different from those of acidic PEMFCs:

* To whom correspondence should be addressed. E-mail: j.varcoe@surrey.ac.uk.
† Department of Chemistry.
‡ MSSU, School of Engineering.

10.1021/jp064898b CCC: $33.50
Published on Web 09/21/2006

TABLE 1: Physical Properties of the AAEM and the Nafion-115 PEM Used in This Study[13]

	ionic functional group	IEC[a]/(mmol of OH^- or H^+ g^{-1})	$t_{wet}/\mu m$	$t_{RH=100\%}/\mu m$	$t_{dry}/\mu m$	WU[b]/%	λ[c]	σ[d]/(S cm^{-1})	r[e]/(Ω cm^2)	MeOH permeability[f]/(cm^2 s^{-1})
Nafion 115	$-SO_3^-H^+$	0.93 ± 0.07	153 ± 3	148 ± 3	121 ± 3	40 ± 2	24 ± 2	0.09 ± 0.02	0.17 ± 0.05	$(1.9 \pm 0.9) \times 10^{-6}$
AAEM	$-N^+(CH_3)_3OH^-$	1.14 ± 0.02	153 ± 4	153 ± 2	133 ± 4	32 ± 2	16 ± 1	0.014 ± 0.002	1.1 ± 0.1	$(0.5 \pm 0.3) \times 10^{-6}$

[a] Ion-exchange capacity of fully dehydrated membrane/(mmol of conductive species g^{-1} of dry ionomer). [b] Water uptake $= 100\% \times (m_{hyd} - m_{dry})/m_{dry}$, where m_{hyd} = mass of the fully hydrated membrane and m_{dry} is the mass of the fully dehydrated membrane. [c] Molecules of H_2O per OH^- or H^+ ions in the fully hydrated membrane. [d] Ionic conductivity at 50 °C in a static relative humidity (RH) = 100% atmosphere. [e] Corresponding area resistance at 50 °C in a static RH = 100% atmosphere. [f] Measured using the method and apparatus described by Nasef et al.[20]

(1) The conducting ions now move from the cathode (where they are generated) to the anode.

(2) H_2O is now produced at the anode.

(3) H_2O is now a stoichiometric reactant at the cathode.

An important physical insight into the primary performance limitation of alkaline membrane fuel cells was gained as an unexpected outcome of the research presented in this paper; this limitation originates in this fundamental change in water mass balance.

This study constitutes, to the best of our knowledge, the first investigation into the performances (over the short term) of commercially available preformed Ag/C- and Au/C-based cathodes in metal−cation−free alkaline membrane fuel cells. The most pressing research challenges relating to catalyst electrochemical characterization and improved performances in alkaline polymer membrane systems are identified. Studies into the longer-term stability of these electrodes and AAEMs in alkaline membrane fuel cells are ongoing and will be reported in due course.

2. Experimental Methods

Ex Situ Physical Characterization of the Alkaline Membrane. The authors have conducted extensive work into the development of radiation-grafted AAEMs that are acceptable for application in fuel cells.[17,18] The AAEM selected for use in this study has been fully characterized using techniques that have been previously described in detail[13] and is that evaluated in a recent communication.[15] The physical properties of this AAEM that are of direct relevance to this study are summarized in Table 1. This membrane was selected as the fully hydrated thickness is identical to that of Nafion-115, which was used as a PEM benchmark and solid-state-acid comparison. For conciseness the details on the AAEM synthetic methodology and physical characterization will not be repeated here but are readily available in the references above.

Electrode Supply and Characterization. Prefabricated electrodes were purchased from E-Tek division of PEMEAS (Somerset, NJ) and contained the carbon-supported catalysts described below, carbon cloth backing layers, and PTFE (undisclosed proprietary loadings) as catalyst layer binding material: Nafion binder was intentionally not ordered in view of the intended application in alkaline-MEAs. All anode electrodes contained Pt/C (20% mass, 0.5 mg_{Pt} cm^{-2}) while the cathodes contained either the same Pt/C catalyst, Ag/C (60% mass, 4 mg_{Ag} cm^{-2}), or Au/C (60% mass, 4 mg_{Au} cm^{-2}); the higher metal loadings for the Ag and Au electrodes were selected in response to the previously reported lower specific activities of Ag particles compared to Pt particles.[19] The particle size distributions of the metal catalysts in these electrodes were determined using transmission electron microscopy (TEM, Phillips CM200, operated at 200 keV); the samples were prepared by scraping the catalysts from the electrode support and ultrasonically dispersing them in methanol for deposition onto standard copper grids.

Fabrication of the Membrane Electrode Assembly. Directly before preparation of the AAEM-MEAs used for fuel cell testing, the AAEMs were converted to the OH^- form, from the stored Cl^- form, by immersion in aqueous KOH (1 mol dm^{-3}) for 1 h (with two changes of solution during this immersion period to ensure complete ion exchange). The electrodes (25 cm^2) were coated with a water insoluble alkaline interface polymer as previously reported:[15] each electrode was coated with 0.27 ± 0.02 mg cm^{-2} poly(vinylbenzyl chloride) (Aldrich, U.K.) using a spray gun and ethyl acetate as solvent; to form the cross-linked (water insoluble) alkaline interface polymer, the treated electrodes were then immersed in *N*,*N*,*N*′,*N*′-tetramethylhexane-1,6-diamine (Acros Organics, U.K.; toxic) for 12 h at room temperature, washed with water, and ion-exchanged to the OH^- form using the procedure above. Cross-linked anion-exchange materials produced using *N*,*N*,*N*′,*N*′-tetramethylhexane-1,6-diamine are reported to have enhanced thermal stability when in the alkali compared to other diamines such as *N*,*N*,*N*′,*N*′-tetramethylethane-1,6-diamine.[21] The MEAs were fabricated by pressing the relevant electrodes to the AAEM with 200 kg cm^{-2} force at 100 °C for 3 min. Before preparation of the Nafion-MEAs (benchmarking), the Nafion-PEM was subjected to the usual aqueous H_2O_2 and H_2SO_4 boiling treatment.[22] The electrodes were coated with commercially available dispersions of Nafion (Aldrich, 5% mass dispersed in water and low aliphatic alcohols) and dried in air to constant mass; loadings of 0.55 mg cm^{-2} Nafion were applied. Acidic MEAs were fabricated by pressing the relevant electrodes to the Nafion-PEM with 120 kg cm^{-2} force at 135 °C for 3 min. The Nafion- and AAEM-MEAs were stored in water until required.

Fuel Cell Testing. Fuel cell testing was conducted with an Arbin Instruments (College Station, TX) fuel cell test station (FCTS). The MEAs were mounted in a 5 × 5 cm test fixture containing graphite blocks with machined triple serpentine flow channels (1 mm channel width, 1 mm channel height, 1.5 mm rib width) and gold-coated current collector plates. The test fixture was assembled with retaining bolts tightened to a torque of 5.5 N m. Fuel cell testing was conducted at a fuel cell temperature of 50 °C with H_2 and O_2 gases (laboratory grade, BOC) supplied at 2 dm^3 min^{-1} flow rates and either relative humidity (RH) = 100 ± 4% (dew point temperature = 50 ± 1 °C) or RH = 82 ± 4% (dew point temperature = 46 ± 1 °C); the gas lines between the dew point humidifiers and the fuel cell fixture were heated at 10 °C more than the set dew point to minimize condensation in the supply pipes. These gas flows correspond to high gas stoichiometries ($\lambda_{O_2} = 23$ and $\lambda_{H_2} = 11.5$ at 1 A cm^{-2}) and water stoichiometries at the cathode ($\lambda_{H_2O} = 1.6$ and 1.3 at 1 A cm^{-2} for the dew points of 50 and 46 °C respectively, calculated assuming no back-transport of water from the anode to the cathode). These high stoichiometries were deliberately chosen in anticipation of minimizing mass transport interferences to facilitate comparison of electrocatalytic performances of the different MEAs; however, as indicated in later discussions, even under these conditions mass transport phe-

nomena substantially limited the performances produced. The fuel cell temperature of 50 °C was selected to ensure minimal thermal degradation of the alkali polymeric materials during testing; current alkali anion-exchange materials containing β-hydrogen atoms (as in the interface alkaline polymer used in this study)[15] exhibit acceptable thermal stability only when kept below 60 °C (as found for numerous anion-exchange membranes and resins).[23,24] Cell voltage (V_{cell}/V) and power density (P_{cell}/(mW cm^{-2})) vs current density (i/(mA cm^{-2})) steady-state polarization curves were collected under galvanostatic control (constant reaction rates) using the FCTS's integral electronic load with data points being recorded after V_{cell} equilibrated to a constant potential (normally 5−10 min); before the i/V_{cell} curves were recorded, each MEA was "conditioned" by operating at high i (potentiostatic cell discharge at 50 mV) until the current density had stabilized at a constant value (1−2 h were required for the AAEM-MEAs to fully hydrate under this conditioning regime). For validation, the i/V_{cell} curve of the AAEM|Ag/C MEA was also recorded using a calibrated Solartron Analytical (Farnborough, U.K.) 1480 mulistat battery tester in addition to the FCTS electronic load; an excellent match was observed. Current densities are referred to the geometric area of the electrodes (25 cm^2).

In Situ Electrochemical Impedance Spectroscopy. Electrochemical impedance spectroscopy (EIS) is the technique of choice that is used to obtain information on separate voltage loss phenomena that are distinguishable by differing relaxation times.[25] In situ impedance spectra were recorded immediately after each point on each i/V_{cell} direct current (dc) curve using a Solartron Analytical 1260 frequency response analyzer operating in conjunction with a 1287 potantiostat/galvanostat. The 1260/1287 instruments were connected to the fuel cell fixture's current collectors in parallel to the dc current loop controlled by the electronic load; the 1260/1287 were operated in floating mode to prevent ground loop interferences. The galvanostatically controlled dc currents were pertubated with small-amplitude alternating currents (ac; *not* ac potentials) at frequencies decreasing from 125 kHz to 100 mHz at 9 points decade^{-1}; the resulting ac voltage responses were recorded and the ac impedances calculated at each frequency. The amplitudes of the ac current pertubations at each dc current discharge were controlled at the lowest levels required for noise-free spectra; this ensures minimal nonlinear distortions to the data. Root-mean-square ac current amplitudes up to a maximum of 200 mA were used for most of the MEAs; the lower the gradient, dV_{cell}/di, of the steady-state dc curve (see Figure 4 in the article by Wagner[26]), the higher the applied amplitude. Individual contributing semicircular features in the impedance spectra were fitted to parallel RC equivalent circuits using the fitting routines in the ZView data analysis software (Scribner Associates Inc., Southern Pines, NC); pure capacitive elements were replaced by constant phase elements, justified by the "real-world" system (as indicated in the appropriate sections of the results in Results and Discussion). The high-frequency x-axis intercepts represent the cell internal resistance; these values closely matched the values obtained using the FCTS's integral fast current pulse internal resistance determination capability.

3. Results and Discussion

TEM Analysis of the Catalysts. Figure 1 shows the particle size distribution of the Pt/C catalysts in the commercial electrodes used in this study. The majority of the particles were in the 2−5 nm range as anticipated; there were, however, a small number of larger particles/agglomorates present (the biggest detected with a particle size of 106 nm). TEM analysis (not shown) of the Ag/C and Au/C electrodes gave wide multimodally dispersed particle size distributions in the ranges of 200−2400 nm (mean = 610 nm) and 13−280 nm (mean = 78 nm), respectively. No particles outside the ranges were present. EDX analysis confirmed there was no Ag or Au present in the carbon regions located away from the large non-Pt particles. It is readily evident that the catalytic surfaces available for the ORR are not optimal with these fuel cell electrodes; despite this, such electrodes are those readily available and perform well (see results below).

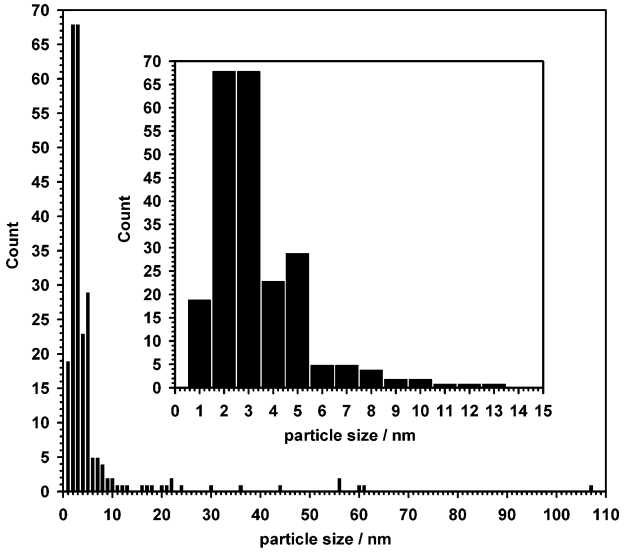

Figure 1. Pt particle size distribution, from TEM measurements, of the commercial 0.5 mg cm^{-2} Pt/C (20% mass) electrodes used in this study.

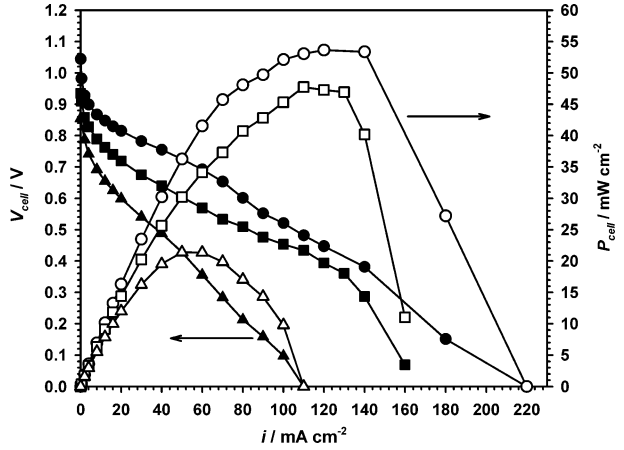

Figure 2. Cell voltage and power density vs current density curves (50 °C, RH = 100%) obtained with AAEM-MEAs containing Pt/C (20% mass, 0.5 mg cm^{-2}) anodes and (●) Pt/C (20% mass, 0.5 mg cm^{-2}), (■) Ag/C (60% mass, 4 mg cm^{-2}), and (▲) Au/C (60% mass, 4 mg cm^{-2}) cathodes. Closed symbols represent V_{cell}, and open symbols represent P_{cell}.

Galvanostatic Characterization of Fuel Cells with MEAs containing Pt/C, Ag/C, and Au/C Cathodes. Figure 2 displays the steady-state beginning-of-life V_{cell} vs i galvanostatic plots for the AAEM-MEAs containing the three differing metal/C cathodes, and Figure 3 shows the equivalent Nafion-MEA performances. The performance of the AAEM|Pt/C MEA (notation membrane|cathode—all anodes are Pt/C|) was poor compared to the equivalent Nafion|Pt/C MEA. The reproducibility of the performances of the AAEM|Pt/C MEA is demonstrated as the performances observed in this study match

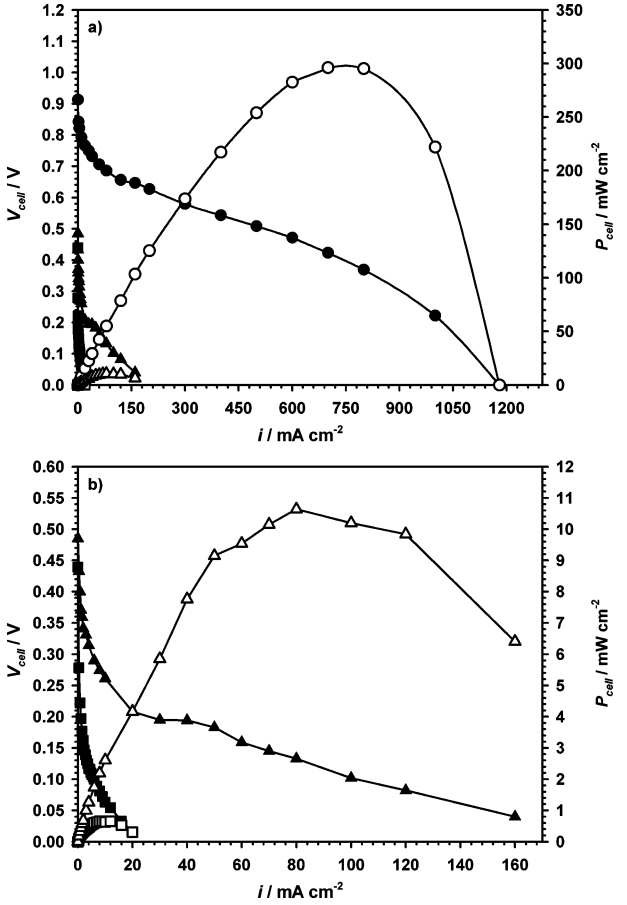

Figure 3. (a) Cell voltage and power density vs current density curves (50 °C, RH = 100%) obtained with Nafion-MEAs containing Pt/C (20% mass, 0.5 mg cm^{-2}) anodes and (●) Pt/C (20% mass, 0.5 mg cm^{-2}), (■) Ag/C (60% mass, 4 mg cm^{-2}), and (▲) Au/C (60% mass, 4 mg cm^{-2}) cathodes. (b) Rescaled curves showing the Ag/C and Au/C performances in detail. Closed symbols represent V_{cell}, and open symbols represent P_{cell}.

those previously reported with a comparable AAEM-MEA (Figure 1 in ref 15; MEA composed of the same AAEM and electrodes and tested under identical conditions). The open circuit voltage (V_{ocv}) (Table 2) is >100 mV higher for the AAEM|Pt/C MEA than the Nafion equivalent, which is indicative of superior electrocatalysis at high pH and/or substantially decreased gas crossover. The peak power performance of the AAEM|Ag/C MEA, despite the poor Ag particle size distribution, was only slightly lower (89%) than the AAEM|Pt/C MEA; the peak power of the AAEM|Au/C MEA was lowered by a factor of 2. The above is in stark contrast with the equivalent Nafion-MEAs, where the peak power and V_{ocv} performances decrease dramatically when Ag/C or Au/C replace the Pt/C in the cathode (2 and 3.6% of the performance obtained with the Pt/C cathode, respectively). This is a significant result and demonstrates that these types of non-noble catalysts are only viable in low-temperature membrane fuel cells operating in a high-pH regime. A previous study by Chatenet et al. also reported the comparable ORR performances of Ag and Pt in alkaline media, an observation that fully supports the data obtained in this study.[27]

For investigative purposes, the AAEM|Ag/C and AAEM|Au/C fuel cells were operated in reverse, with the non-noble catalysts at the anode and Pt/C at the cathode; however, limiting current densities of <0.01 and <1.25 mA cm^{-2}, respectively, were obtained indicating poor hydrogen oxidation reaction (HOR) characteristics on the non-Pt metals.

The Tafel plots for the AAEM- and Nafion-MEAs are presented in Figure 4a; the internal resistances used to construct these plots are presented in Figure 4b. The Tafel slopes (Table 2) of the MEAs (ignoring the poorly performing Nafion|Ag/C and Au/C MEAs) decrease in the order AAEM|Au/C ≫ AAEM|Ag/C ≈ AAEM|Pt/C > Nafion|Pt/C; the Tafel slopes, *b*, give an indication of the number of electrons involved in the reaction mechanism via the following equation:[28,29]

$$b = 2.3\frac{RT}{\alpha nF} \tag{4}$$

where R is the gas constant (8.3145 J K mol^{-1}), T is the thermodynamic temperature (K), F is Faraday's constant (96 485.3 C mol^{-1}), α is the charge-transfer coefficient, and n is the number of electrons transferred in the rate-determining step. The considerably higher value of b for the AAEM|Au/C (bearing in mind the anodes are identical in all MEAs) is an initial indication that a different mechanism is operating. The extent of ORR is very sensitive to the structure and particle size of the Au catalysts;[1] 4e$^-$ reduction is predominant on the Au(100) facets.[4] The higher b values may well indicate a 2e$^-$ reduction mechanism for these commercial Au/C cathodes; however, further experimental evidence is required to confirm the precise ORR mechanism that is operating. Higher Tafel slopes can also result if diffusion of O_2 in the flooded catalyst agglomerates is controlling the kinetics,[25] though this is not considered relevant here for such a large increase in b.

The onsets of the deviations from linearity of the Tafel plots occur at significantly lower current densities with the AAEM-MEAs (as low as 20−30 mA cm^{-2}) compared to the Nafion|Pt/C MEA (>600 mA cm^{-2}). These deviations either originate from a change in mechanism at different potentials or mass transport overpotentials; the latter is consistent with the results of impedance studies presented below. This early onset of mass transport limitations is surprising considering the deliberate use of high reactant stoichiometries; this limitation explains the poorer AAEM|Pt/C MEA performance compared to the acidic equivalent. The significant shift to higher *ir*-corrected cell potentials at low current densities in the Tafel plots of the AAEM|Pt/C MEA as compared to the Nafion|Pt/C analogue is symptomatic of higher apparent exchange current densities, j_o (normalized with geometric electrode area), at high pH. However, the two membranes may exhibit different gas permeabilities, and caution is therefore required in such direct comparisons.

The cell resistances were more independent on current, at these relatively low current densities, for the Nafion-MEAs when compared to the AAEM-MEAs; a distinct lowering of the area resistances, r, were observed at high i's for the latter. The Nafion|Pt/C MEA was lower in resistance as compared with the AAEM|Pt/C MEA (as expected from ex situ resistance determinations); however, the Nafion-MEAs were a factor of 3 higher in resistance in situ to the operating fuel cell than expected from the ex situ observations, while the r values were generally lower than expected for the AAEM-MEA at higher current densities. This shows that care must be taken with applying ex situ membranes resistances to fuel cell performances and that recording in situ internal resistances at each current density, as in this study, is vital. It is well-known that collapse of the ionic clusters and channels in Nafion takes place on dehydration, as occurs in hot-pressing, and recovery of the fully hydrated state occurs only on high-temperature (80 °C) treatment in water;[30] the Nafion-MEAs in this study were only soaked in water after fabrication to be consistent with the procedure for

TABLE 2: Selected Electrochemical Properties of the AAEM- and Nafion-MEAs

MEA	V_{ocv}/V	Tafel slope[a]/(mV dec^{-1})	Tafel slope[b]/(mV dec^{-1})	R_{p1}[c]/Ω
Pt/C|AAEM|Pt/C (RH = 100%)	1.04	86 ± 2	86 ± 1	0.024 ± 0.002
Pt/C|AAEM|Ag/C (RH = 100%)	0.94	84 ± 7	106 ± 11	0.05 ± 0.01
Pt/C|AAEM|Au/C (RH = 100%)	0.86	155 ± 5	324 ± 5 or 173 ± 8[d]	0.09 ± 0.02
Pt/C|AAEM|Pt/C (RH = 82% at cathode)	1.08	95 ± 4		0.029 ± 0.002
Pt/C|AAEM|Pt/C (RH = 82% at anode)	1.10	96 ± 5		0.030 ± 0.002
Pt/C|Nafion|Pt/C (RH = 100%)	0.91	69 ± 1	71 ± 1	
Pt/C|Nafion|Ag/C (RH = 100%)	0.44	164 ± 5	161 ± 17	
Pt/C|Nafion|Au/C (RH = 100%)	0.49	118 ± 3	106 ± 36	

[a] From Tafel plots constructed from *ir*-corrected-V_{cell} vs log *i* galvanostatic data (Figure 4). [b] From Tafel plots constructed from *ir* -corrected-V_{cell} vs log$(R_{ct})^{-1}$ EIS data (Figure 6). [c] The potential independent high-frequency feature observed in the EIS spectra of the AAEM-MEAs (see Figure 5 and related discussions in the main text). [d] There appeared to be two slopes at high *ir* -corrected potentials; the origin of this is currently unknown.

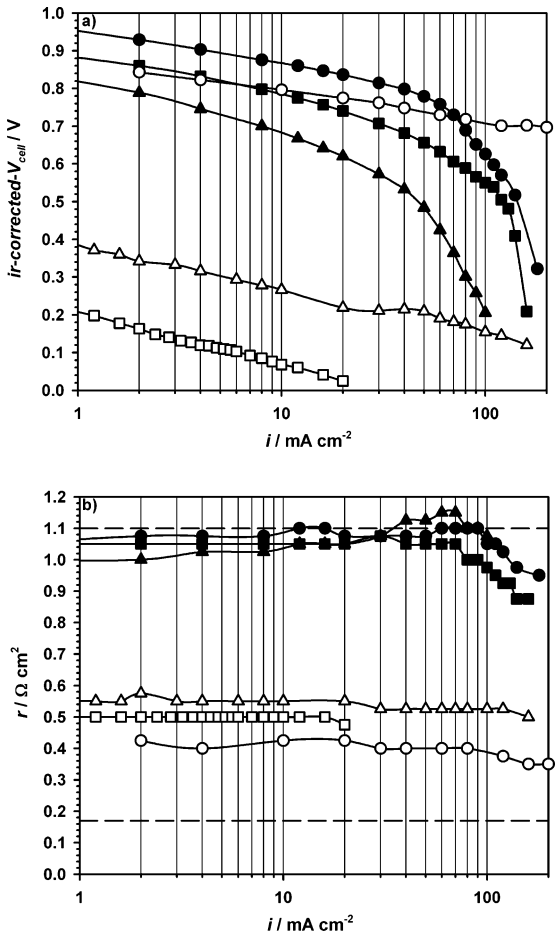

Figure 4. (a) Tafel plots and (b) area resistances (EIS high frequency *x*-axis intercepts) of all MEAs at 50 °C and RH = 100% (open symbols = Nafion-MEAs and closed symbols = AAEM-MEAs): (●) Pt/C(20%mass, 0.5 mg cm^{-2}), (■) Ag/C (60% mass, 4 mg cm^{-2}), and (▲) Au/C (60% mass, 4 mg cm^{-2}) cathodes. The horizontal dashed lines represent the ex situ area resistances (Table 1).

the production of the AAEM-MEAs. The ex situ conductivity measurements were conducted in static atmospheres of RH = 100%, while the in situ resistance measurements are recorded with the MEAs in dynamic environments consisting of flowing atmospheres and significant ion conduction (and therefore water transport) within the membranes; the expectation of differing material resistances in these diverse situations is not unreasonable.

Of relevance to alkaline membrane direct methanol fuel cells (AAEM-DMFCs) is the methanol permeability data presented in Table 1. Whereas the AAEMs have lower conductivities than Nafion, they also have lower methanol permeabilities; thinner membranes could therefore be used to offset the conductivity disadvantage. However, despite this, power densities < 0.25 mW cm^{-2} were obtained when the Au/C and Ag/C electrodes were applied to the cathodes of AAEM-MEAs containing 4 mg cm^{-2} Pt black anodes which were supplied with aqueous methanol (2 mol dm^{-3}) in an alkaline membrane direct methanol fuel cell arrangement. A peak power density of 0.8 mW cm^{-2} was obtained with an MEA containing Pt black at both of the cathodes and cathodes, while switching to 4 mg cm^{-2} PtRu anodes with 4 mg cm^{-2} Pt black cathodes resulted in a still limited 1.5 mW cm^{-2} at 50 °C.[18] It is evident from these observations that considerable work is required in order to obtain alkaline direct alcohol fuel cell performances on a par with those containing Nafion-PEMs (>250 mW cm^{-2} have been obtained in state-of-the-art Nafion DMFC systems).[31]

In Situ Impedance Spectroscopy. The EIS spectra of the Nafion-MEAs obtained in this study were comparable to the spectra in numerous in situ EIS studies of PEMFCs.[30−34] The reported features characteristic of these PEMFC spectra are (1) a linear, near 45°, potential-independent distributive element at high frequencies, sometimes with a discernible inflection[30] (as part of a potential-independent high-*f* semicircular element), that are attributed to proton resistance/transport in the porous electrodes; (2) a medium-*f* semicircular feature that decreases with increasing *i* representing a charge-transfer resistance (R_{ct}) in parallel to the electrode double layer capacitance (C_{dl}) [parallel *RC* circuit]; and (3) a low-*f* depressed semicircular element that only appears at higher *i*'s and grows with increasing *i* (the origins of this are a source of debate in the literature and are attributed to either (a) restricted oxygen diffusibility through the flooded pores in the porous cathode electrode structures combined with limited water transport in the membranes[30] or (b) an additional nonnegligible HOR activation overpotential in the anodes due to low H^+ mobilities and/or inhibition of the reactant sites caused by drying out of the ionomer surrounding the catalysts).[32]

The main difference between the spectra of the Nafion-MEAs in this study and those discussed above (which mainly used air rather than O_2 at the cathode) was the lack of any significant low-*f* semicircular elements: this was expected considering the high stoichiometries of pure O_2 used in this study[34] and that reactant diffusion limitations were not observed in the Tafel plots until very high current densities. The lack of a clearly discernible inflection in the high-*f* linear distributed element is suggestive of relatively uninhibited proton transport in the electrode structures, leading to minimal loss of ORR activity due to limited proton availability.[30]

The EIS spectra of the AAEM-MEAs at 50 °C and RH = 100% at *i* = 16 and 70 mA cm^{-2} are presented in Figure 5; these current densities are respectively below and above the levels where the mass transport limitations manifested themselves in the dc Tafel plots (Figure 4). Potential-independent

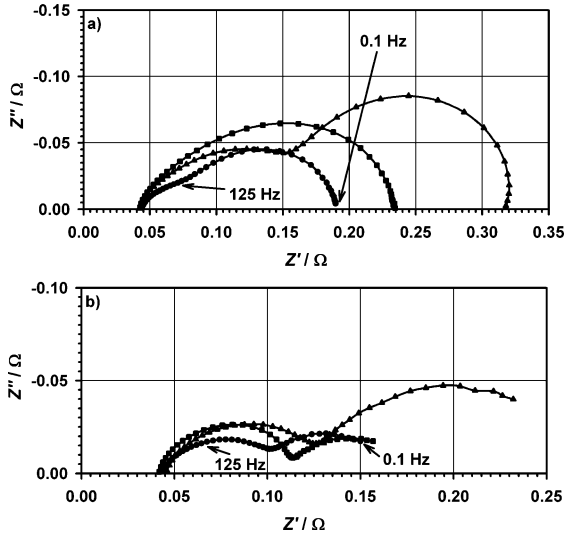

Figure 5. In situ EIS spectra at (a) 16 and (b) 70 mA cm^{-2} galvanostatic current densities of the AAEM fuel cells at 50 °C and RH = 100% containing the following cathodes: (●) Pt/C (20% mass, 0.5 mg cm^{-2}), (■) Ag/C (60% mass, 4 mg cm^{-2}), and (▲) Au/C (60% mass, 4 mg cm^{-2}). Selected frequencies for the AAEM fuel cell containing the Pt-containing MEA are shown. Z' is the real component of the impedance cell impedance vector, $\mathbf{Z}(f)$, while Z'' is the imaginary component.

high-*f* semicircular features (parallel $R_{p1}C_{p1}$ equivalent circuit) were identified, and equivalent circuits were fitted, with constant phase elements (C_{cpe}) replacing pure capacitive elements because of the porous, distributed nature of the electrodes. The values of R_{p1} from these fits are presented in Table 2; these values should be considered tentative (apart from those obtained with the AAEM|Au/C MEA) as these high-*f* impedance features were significantly masked, particularly at low current densities, by the larger medium-*f* parallel $R_{ct}C_{dl}$ impedance. As this high-*f* EIS characteristic corresponds to restricted ionic transport in the porous electrode structures, it is evident that higher OH^- impedances inside the electrode structures are present for the AAEM-MEAs when compared to the H^+ resistances in the electrodes of the Nafion-MEAs. The larger value for the Au/C electrodes indicates an increased ionic resistance in the electrodes with this particular metal. As a control experiment an AAEM|Pt/C MEA was constructed without the ionomer interface polymer: the magnitude of this high-*f* impedance increases substantially, thereby validating the above assignment. These higher OH^- ionic resistances are consistent with the differences between H^+ and OH^- conductive materials (the latter species possesses intrinsically lower ion mobilities) as exemplified by the membrane resistances presented in Table 1.

The medium-*f* $R_{ct}C_{dl}$ parallel elements (order of magnitude dependence on *ir*-corrected-V_{cell}) were equivalent-circuit-fitted (values of R_{ct} presented in Figure 6) only when clearly discernible from the high-*f* and low-*f* spectral features (i.e. more than 2 orders of magnitude difference in time constants, $t_c = RC$). The expected exponential drop in R_{ct} with *i* was observed. The plots of *ir*-corrected-V_{cell} vs $\log(R_{ct}^{-1})$ constitute the EIS counterpart of the Tafel plots presented in Figure 4.[25,33] The ac Tafel slopes from Figure 6b are presented in Table 2 and, apart from the complex response of the AAEM|Au/C MEA, were in good agreement with the Tafel data obtained from the dc steady-state iV_{cell} curves. Again, the shift to higher *ir*-corrected-V_{cell} values for the AAEM|Pt/C (compared to the Nafion counterpart) confirms a higher apparent j_o (mA cm_{geo}^{-2}) for the alkaline-MEA. These ac Tafel plots can be used to obtain approximate

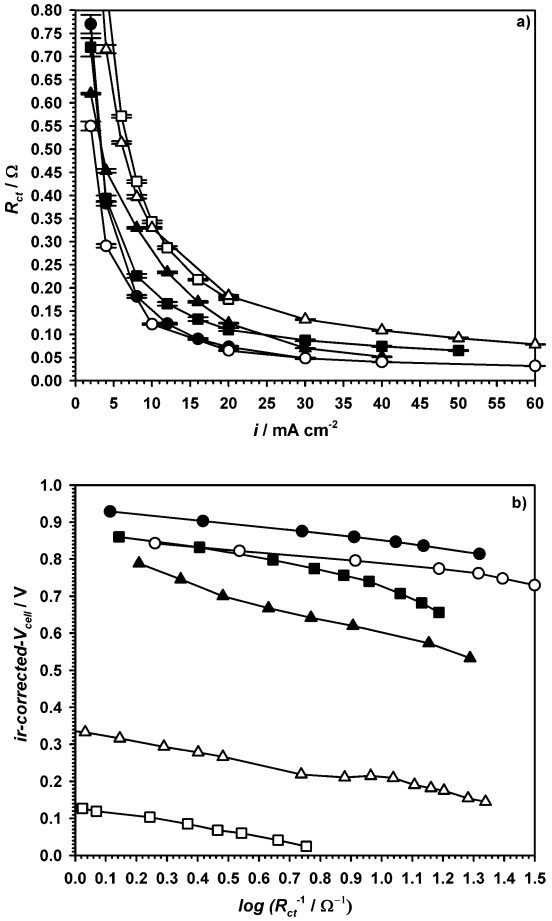

Figure 6. Plots of the dependencies for all MEAs at 50 °C and RH = 100% (open symbols = Nafion-MEAs and closed symbols = AAEM-MEAs) linking the charge-transfer resistances (R_{ct}) and (a) current densities and (b) *ir*-corrected cell voltages: (●) Pt/C (20% mass, 0.5 mg cm^{-2}), (■) Ag/C (60% mass, 4 mg cm^{-2}), and (▲) Au/C (60% mass, 4 mg cm^{-2}) cathodes.

values for the exchange current densities for the cathodes.[33] If the *ir*-corrected-V_{cell} is assumed to be $V_{cathode}$, then

$$V_{cathode} = E_o - b \log(R_{ct}^{-1}) \quad (5)$$

$$E_o = E_{eq} - b \log(R_{ct,o}) \quad (6)$$

where E_{eq} for $H_2 + {}^1/_2O_2 \rightarrow H_2O$ at 50 °C was taken to be 1.21 V.[35] The intercepts at $\log(R_{ct}^{-1}) = 0$ yielded $R_{ct,o}$ values for the Nafion|Pt/C, AAEM|Pt/C and AAEM|Ag/C MEAs of 57.0 $\times 10^3$, 1.36 $\times 10^3$, and 1.43 $\times 10^3$ Ω, respectively. These values can be converted to apparent exchange current densities ($j_{o,geo}$, based on the geometric area of the electrodes and not taking into account the true surface area of the metal catalyst particles or the catalyst utilizations) using the following equation:[26]

$$j_{o,geo} = \frac{RT}{nFR_{ct,o}A_{geo}} \quad (7)$$

Values of 2.0×10^{-8}, 8.2×10^{-7} and 7.8×10^{-7} A cm_{geo}^{-2} at 50 °C were obtained for the Nafion|Pt/C, AAEM|Pt/C, and AAEM|Ag/C MEAs, respectively. Obviously these values are semiquantitative considering the crudity of the linear regression (the low currents used were at the limit of the electronic load): however, the values do suggest that there is at least an order of magnitude improvement with the Pt/C electrodes when moving from low to high pH and that Ag/C (60% mass, 4 mg cm^{-2})

cathodes have comparable performances to the Pt/C (20% mass, 0.5 mg cm^{-2}) cathodes in the AAEM-MEAs, despite the poorer Ag particle size distribution. The value obtained for the Nafion|Pt/C MEA is similar in magnitude to previous values reported in the literature.[36]

Exchange current densities based on the actual surface areas would be useful. However, the broad multimodal particle size distributions of these catalysts prevent meaningful values being obtained in this study. In situ catalyst utilizations in these alkaline-MEAs are also currently unknown, and significant future method development is required to allow such determinations. Catalyst utilizations in Nafion-MEAs are usually determined using in situ cyclic voltammetry in driven-cell mode,[2] where the O_2/air supply at the cathode is replaced with N_2 and the anode, with H_2 supply, constitutes a joint counter and *quasi* reference electrode; the electrochemical area of the cathode catalysts in the MEA are determined from the hydrogen adsorption/desorption peaks in the voltammograms (H_2 generated from the H^+ available in the membrane and acidic binder). This is not the case with alkaline-MEAs, where OH^- is the conductive species from cathode to anode; O_2 is required at the cathode for facile generation of the OH^- ions (part of the redox couple), and the exchange current density (i.e. reversibility) of the hydrogen oxidation reaction in alkali is lower than in acid (relevant for dynamic hydrogen electrodes acting as a joint reference and counter).[37] This latter point is also important in relation to the fuel cell performance curves and Tafel plots above; care must be taken with assigning the kinetic overpotentials purely to the ORR at the cathode. Even at low pH, the overpotential of the HOR can become significant at high current densities.[38] However, with the low current densities achieved with the AAEM-MEAs, the assumption that the HOR kinetic overpotentials are considerably less than the ORR overpotentials is reasonable. The same Pt/C anodes and same membrane were used for all AAEM-MEAs, so comparative differences in the performance curves can only be attributed to the varying cathode performances.

Figure 5b shows the in situ EIS spectra at higher current densities, where the low-*f* depressed semicircular features characteristic of reactant mass transport limitations are well-established. Note that the medium-*f RC* elements overlap to an extent with the high-*f RC* elements for the AAEM|Pt/C and AAEM|Ag/C MEAs. The medium-*f RC* element overlaps significantly with the low-*f* semicircular feature in the AAEM|Au/C case, making fitting of this latter feature difficult until high current densities. These low-*f* depressed semicircles could not be modeled accurately using parallel *RC* equivalent circuits, so CPE's were used for fitting (again justified by considering the distributed nature of these diffusion-based impedances). The results from fitting for all AAEM-MEAs are presented in Figure 7, and the following relates only to the data where both electrodes are supplied with RH = 100% gases. The current densities where the low-*f* feature becomes manifest for the AAEM|Pt/C and AAEM|Ag/C MEAs match the current densities in the Tafel plots in Figure 4 at which nonlinear behavior begins. This confirms that these low-*f* features are associated with a mass transport phenomenon. The R_{p2} values for the AAEM|Pt/C MEA initially increase with current density and then begin to decrease; this behavior has not been reported for EIS spectra of PEMFCs and appears unique to AAEM-MEA-based fuel cells.

Fuel Cell and EIS Studies with Gas Supplies of Lowered Relative Humidity. As mentioned previously, these early onset mass transport performance limitations are surprising considering the high stoichiometries of the reactants used in this study. Understanding the origin of these limitations is a priority as they constitute the primary cause of the lowered performances observed for these alkaline membrane fuel cells compared to the Nafion|Pt/C analogues. The obvious candidate for these mass transport overpotentials is water: the preformed electrodes contain hydrophobic PTFE as a binding material, and, unlike with PEMFCs, water is a stoichiometric reactant at the cathode (eq 2). Most of the water supplied in the gas flows would be expected to flow out of the fuel cell outlets when considering the hydrophobic nature of the electrodes. The hypothesis is that, even though the water is being supplied at a superstoichiometric rate to the cathode, the water is not getting to the reaction zones in an efficient manner. To examine this, the AAEM|Pt/C MEA was tested with reduced humidity at the cathode. The corresponding iV_{cell} plots and Tafel plots, along with those obtained with reduced anode humidity, are shown in Figures 8 and 9, respectively. There are small increases in cell resistance and R_{p1} (Table 2) with the lowered humidity at each electrode, indicating slightly decreased ionic conductivities in the membrane and slightly increased restrictions to ionic transport in

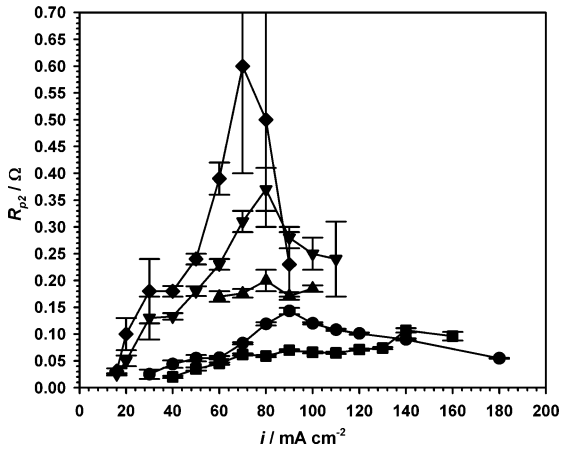

Figure 7. Plots showing the current dependency of the width of the low-*f* depressed semicircular features in the high *i* EIS spectra of the AAEM-MEAs: (●) Pt/C (20% mass, 0.5 mg cm^{-2}) at RH = 100%, (■) Ag/C (60% mass, 4 mg cm^{-2}) at RH = 100%, (▲) Au/C (60% mass, 4 mg cm^{-2}) at RH = 100%, (▼) Pt/C (20% mass, 0.5 mg cm^{-2}) with cathode humidity reduced to RH = 82% and anode at RH = 100%, and (◆) Pt/C (20% mass, 0.5 mg cm^{-2}) with anode humidity reduced to RH = 82% and cathode at RH = 100%.

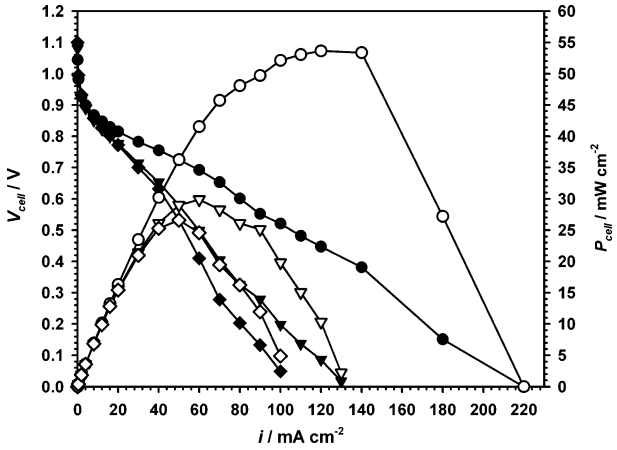

Figure 8. iV_{cell} curves for the AAEM|Pt/C MEA at 50 °C: (●) RH = 100% at both electrodes, (▼) cathode reduced to RH = 82% and anode at RH = 100%, and (◆) anode reduced to RH = 82% and cathode at RH = 100%. Closed symbols represent V_{cell}, and open symbols represent P_{cell}.

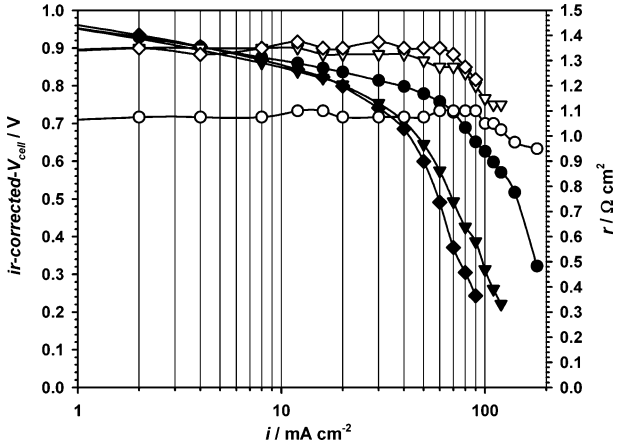

Figure 9. The Tafel plots for the AAEM|Pt/C MEA at 50 °C: (●) RH = 100% at both electrodes, (▼) cathode reduced to RH = 82% and anode at RH = 100%, and (◆) anode reduced to RH = 82% and cathode at RH = 100%. Closed symbols represent the *ir*-corrected-V_{cell}, and open symbols represent the area resistances.

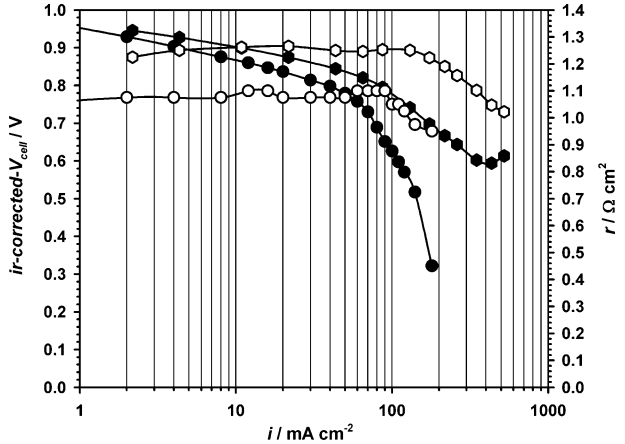

Figure 10. Tafel plots for at 50 °C and RH = 100% with the (●) AAEM|Pt/C MEA (t_{wet} = 153 ± 4 μm) in this study and (⬣) AAEM|Pt/C MEA with the thinner AAEM (t_{wet} = 51 ± 2 μm) reported in ref 18. Closed symbols represent the *ir*-corrected-V_{cell}, and open symbols represent the area resistances.

the electrodes, respectively. However, these small resistance increases do not wholly explain the substantial decrease in the power performances with lowered humidity. The Tafel plot of the AAEM|Pt/C MEA with reduced humidity at the cathode reveals an onset of nonlinearity, with concomitant appearance of the low-*f* impedance in the EIS spectra (Figure 7), at a lower current density; the magnitudes of R_{p2} at each current density are also substantially increased relative to those obtained under RH = 100% conditions. These mass transport manifestations would have decreased if the root cause were inhibited gas transport to the reaction zones due to liquid water in the porous electrode structures. Inefficient mass transport of water to the reaction zones in the cathode is therefore likely to be the primarily cause of performance loss in AAEM-based fuel cells with the commercial electrodes used.

Contrary to expectation, the magnitude of the mass transport losses was higher with reduced anode humidity rather than reduced cathode humidity (evident in Figures 7−9). Back-transport of water from the anode (where it is generated—see eq 1) to the cathode can be anticipated, so a lowering of humidity at the anode was predicted to lead to a small drop in performance. This effect was not expected to be larger than that when the humidity was lowered at the cathode. Tafel plots (Figure 10) constructed from the i/V_{cell} curves, presented in Figure 2 in a recent communication,[18] using the same Pt/C alkaline electrodes and testing conditions but a *thinner* AAEM (51 ± 2 μm) of similar area resistance, showed that the magnitudes of mass transport losses were lower with this thinner membrane. A peak power density of 90 mW cm^{-2} was obtained with the MEA containing this thinner AAEM as a direct result of the reduced mass transport overpotential (now up to 30% of the power performance obtained with the Nafion|Pt/C MEA); this was despite a lowering of V_{ocv} from 1.04 to 0.98 V (higher gas crossover with the thinner AAEM). This is clear evidence for the importance of water back-transport from the anode to the cathode reaction zones, which is facilitated with the use of thinner membranes. The Tafel slope, *b*, at low current densities is slightly improved with the thinner AAEM; this indicates that even at low−medium current densities mass transport interferences were not negligible for the thicker AAEM-MEA.

The complexity of the water transport and membrane hydration characteristics is evident when considering the following observations:

1. The significant performance losses with reduced humidity at the anode.

2. The reproducible lowering of cell resistance at higher current densities.

3. The decrease in the magnitudes of R_{p2} with current density after an initial increase (i.e. a current density can be identified where the R_{p2} values peak).

Observations 2 and 3 above are clearly linked. A detailed examination of Figure 8 reveals that, with AAEM|Pt/C MEAs in each humidity environment, there is a slight increase in the gradient (less negative) of the iV_{cell} curves at high current densities; this occurs after the gradients have already decreased (more negative) due to the onset of mass transport overpotentials. These small relative recoveries in power performance occur at current densities that are concurrent with those where the area resistances of the cell begin to decrease and where the values of R_{p2} peak. This situation is not so clear-cut with the Ag/C and Au/C anodes and does not occur with the Nafion|Pt/C MEA. All of this evidence leads to the following hypothesis concerning the use of these preformed intrinsically hydrophobic electrodes in AAEM-MEAs: a major source of the reactant water at the cathode is back-transport of the water generated at the anode (this is despite the opposing direction OH^- ionic conduction). At higher current densities this back-transport of water leads to an increased membrane hydration (i.e. lowered in situ membrane resistance), which in turn enhances the rate of the back-transport of water from anode to cathode (lowered R_{p2} values). Lowering the RH at the anode supplied with fast (2 dm^{-3} min^{-1}) gas flows leads to facilitated removal of the electrochemically generated water, which consequently reduces the amount of water back-transported to the cathode and increases the mass transport overpotential.

Concluding Remarks

It is evident that currently the AAEM properties are not the main source of fuel cell performance losses in metal−cation−free alkaline membrane fuel cells. Therefore, the following research priorities regarding the application of AAEMs to fuel cells are highlighted: There is a need to maximize the amounts of water transported from the cathode gas to the ORR reaction sites to complement to the water supplied by back-transport from the anode (i.e. modifying the PTFE and/or alkaline ionomer content of the cathodes); a resultant drop in the observed sensitivity of fuel cell performance toward anode humidity

would substantiate the water back-transport hypothesis. Optimization of the electrode architectures (including the anode and with the intention of reducing the loss of electrochemically generated water into the anode gas flow), the particle size distributions of the metal catalysts (to maximize the electrokinetics and utilization of the metal atoms) and the AAEM fuel cell operating conditions are all urgently required for fuel cell performances comparable to state-of-the art PEMFCs.

Acknowledgment. This study was supported financially by the Engineering and Physical Sciences Research Council (Grant GR/S60709/01). Andrew White and Andrew Savage (Solartron Analytical) are also thanked for the numerous and helpful discussions regarding in situ EIS testing of fuel cells.

References and Notes

(1) Wang, B. *J. Power Sources* **2005**, *152*, 1−15.
(2) Gasteiger, H. A.; Kocha, S. S.; Sompalli, B., Wagner, F. T. *Appl. Catal., B* **2005**, *56*, 9−35.
(3) Blizanac, B. B.; Ross, P. N.; Marković, N. M. *J. Phys. Chem. B* **2006**, *110*, 4735−4741.
(4) Kim, J.; Gewirth, A. A. *J. Phys. Chem. B* **2006**, *110*, 2565−2571.
(5) Meng, H.; Shen, P. K. *Electrochem. Commun.* **2006**, *8*, 588−594.
(6) Lima, F. H. B.; Sanches, C. D.; Ticianelli, E. A. *J. Electrochem. Soc.* **2005**, *152*, A1466−A1473.
(7) Coutanceau, C.; Demarconnay, L.; Lamy, C.; Léger, J.-M. *J. Power Sources* **2006**, *156*, 14−19.
(8) Matsuoka, K.; Iriyama, Y.; Abe, T.; Matsuoka, M.; Ogumi, Z. *J. Power Sources* **2005**, *150*, 27−31.
(9) Wagner, N.; Schulze, M.; Gülzow, E. *J. Power Sources* **2004**, *127*, 264−272.
(10) Schulze, M.; Gülzow, E. *J. Power Sources* **2004**, *127*, 252−263.
(11) Varcoe, J. R.; Slade, R. C. T. *Fuel Cells* **2005**, *5*, 187−200.
(12) Agel, E.; Bouet, J.; Fauvarque, J. F. *J. Power Sources* **2001**, *101*, 267−274.
(13) Varcoe, J. R.; Slade, R. C. T. *Solid State Ionics* **2005**, *176*, 585−597.
(14) Danks, T. N.; Slade, R. C. T.; Varcoe, J. R. *J. Mater. Chem.* **2003**, *13*, 712−721.
(15) Varcoe, J. R.; Slade, R. C. T. *Chem. Commun. (Cambridge)* **2006**, 1428−1429.
(16) Sata, T.; Tsujimoto, M.; Yamaguchi, T.; Matsusaki, K. *J. Membr. Sci.* **1996**, *112*, 161−170.
(17) Herman, H.; Slade, R. C. T.; Varcoe, J. R. *J. Membr. Sci.* **2003**, *218*, 147−163.
(18) Varcoe, J. R.; Slade, R. C. T. *Electrochem. Commun.* **2006**, *8*, 839−843.
(19) Demarconnay, L.; Coutanceau, C.; Leger, J.-M. *Electrochim. Acta* **2004**, *49*, 4513−4521.
(20) Nasef, M. M.; Zubir, N. A.; Ismail, A. F.; Dahlan, K. Z. M.; Saidi, H.; Khayet, M. *J. Power Sources* **2006**, *156*, 200−210.
(21) Komkova, E. N.; Stamatialis, D. F.; Strathmann, H.; Wessling, M. *J. Membr. Sci.* **2004**, *244*, 25−34.
(22) Silva, R. F.; De Francesco, M.; Pozio, A. *J. Power Sources* **2004**, *134*, 18−26.
(23) Tomoi, M.; Yamaguchi, K.; Ando, R.; Kantake, Y.; Aosaki, Y.; Kubota, H. *J. Appl. Polym. Sci.* **1997**, *64*, 1161−1167.
(24) Zagorodni, A. A.; Kotova, D. L.; Selemenev, V. F. *React. Funct. Polym.* **2002**, *53*, 157−171.
(25) Paganin, V. A.; Oliveira, C. L. F.; Ticianelli, E. A.; Springer, T. E.; Gonzalez, E. R. *Electrochim. Acta* **1998**, *43*, 3761−3766.
(26) Wagner, N. *J. Electrochem. Soc.* **2002**, *32*, 859−863.
(27) Chatenet, M.; Genies-Bultel, L.; Aurousseau, M.; Durand, R.; Andolfatto, F. *J. Appl. Electrochem.* **2002**, *32*, 1131−1140.
(28) Xie, Z.; Holdcroft, S. *J. Electroanal. Chem.* **2004**, *568*, 247−260.
(29) Wakabayashi, N.; Takeichi, M.; Itagaki, M.; Uchida, H.; Watanabe, M. *J. Electroanal. Chem.* **2005**, 339−346.
(30) Freire, T. J. P.; Gonzalez, E. R. *J. Electroanal. Chem.* **2001**, *503*, 57−68.
(31) Dillon, R.; Srinivasan, S.; Aricò, A. S.; Antonucci, V. *J. Power Sources* **2004**, *127*, 112−126.
(32) Andreaus, B. McEvoy, A. J.; Scherer, G. G. *Electrochim. Acta* **2002**, *47*, 2223−2229.
(33) Ciureanu, M.; Roberge, R. *J. Phys. Chem. B* **2001**, *105*, 3531−3539.
(34) Springer, T. E.; Zawodzinski, T. A.; Wilson, M. S.; Gottesfeld, S. *J. Electrochem. Soc.* **1996**, *143*, 587−599.
(35) Larminie, J.; Dicks, A. *Fuel Cell Systems Explained*; John Wiley & Sons: Chichester, U.K., 2000.
(36) Sena, D. R.; Ticianelli, E. A.; Paganin, V. A.; Gonzalez, E. R. *J. Electroanal. Chem.* **1999**, *477*, 164−170.
(37) Chen, S.; Kucernak, A. *J. Phys. Chem. B* **2005**, *108*, 13984−13994.
(38) Kuhn, H.; Andreaus, B.; Wokaun, A.; Scherer, G. G. *Electrochim. Acta* **2006**, *51*, 1622−1628.